CO_2 emissions from a spark ignition engine operating on natural gas–hydrogen blends (HCNG)

Emilio Navarro [a,*], Teresa J. Leo [b], Roberto Corral [b]

[a] Dept. Motopropulsión y Termofluidodinámica, E.T.S.I. Aeronáuticos, Universidad Politécnica de Madrid, Madrid, Spain
[b] Dept. Sistemas Oceánicos y Navales, E.T.S.I. Navales, Universidad Politécnica de Madrid, Madrid, Spain

The addition of hydrogen to natural gas could be a short-term alternative to today's fossil fuels, as greenhouse gas emissions may be reduced. The aim of this study is to evaluate the emissions and performance of a spark ignition engine fuelled by pure natural gas, pure hydrogen, and different blends of hydrogen and natural gas (HCNG). Increasing the hydrogen fraction leads to variations in cylinder pressure and CO_2 emissions. In this study, a combustion model based on thermodynamic equations is used, considering separate zones for burned and unburned gases. The results show that the maximum cylinder pressure rises as the fraction of hydrogen in the blend increases. The presence of hydrogen in the blend leads to a decrease in CO_2 emissions. Due to the properties of hydrogen, leaner fuel–air mixtures can be used along with the appropriate spark timing, leading to an improvement in engine emissions with no loss of performance.

1. Introduction

Crude oil reserves are not unlimited. In the future, we will have to resort to oil fields that are much more difficult to exploit (higher depths, higher densities), and additional extraction problems will arise. These circumstances will probably require investments in more developed extraction techniques, leading to higher crude oil prices. It is also important to note that demand is increasing more than supply. This is becoming more evident with the development of new economies such as China and India, which will require huge amounts of energy.

On the other hand, growing concern for the environment in all areas of knowledge also affects the engine manufacturing industry. To make engines more environmentally friendly, studies focus on decreasing greenhouse gas emissions to the atmosphere by developing different alternatives to fossil fuels [1–3] and new engine types, such as HCCI [4,5].

Natural gas is regarded as a suitable alternative to other fossil fuels because its combustion features are cleaner and higher proven reserves are available [6,7]. Natural gas has excellent anti-knock properties due to its higher compression ratio, which provides improved efficiency and power. However, its flame propagation rate is low, and its auto-ignition temperature is high.

Hydrogen is postulated as the long-term alternative. While not free, it is abundant in nature and its combustion products are almost harmless. However, most hydrogen is now obtained from fossil fuels, and therefore does not solve the problem of dependency on such fuels. Storage is also an issue because hydrogen is highly explosive and requires large, heavy tanks. Hydrogen has high flame propagation rates, making it easier to ignite, but reduces engine performance compared to fossil fuels [8,9].

An alternative solution, as a transition to hydrogen technology, is natural gas blended with hydrogen, known as HCNG. A combination of the two fuels could overcome the limitations of both pure natural gas and hydrogen.

When experimental or simulation studies on reciprocating engines are carried out, much attention is paid to pollutant CO, HC and NO_x emissions. Nevertheless, although CO_2 is one of the most important greenhouse gases, these emissions are not usually taken into account, and measurements and calculations of CO_2 emissions are omitted from many studies. This is the case of many studies of HCNG mixtures, of which only a few analyse CO_2 emissions. For example, experimental tests are performed by Ma et al. [10] to validate the proposed model, but no other studies are conducted. Park et al. [11] use a model to study NO_x variations with 0%, 5%, 10% and 15% of H_2 in the mixtures. Dimopoulos et al. [12] carry out a thermodynamic analysis where CO and NO_x emissions are analysed with 0%, 10% and 15% H_2 mixtures. Tests with mixtures containing 0% and 29% H_2 are performed by Bysveen [13], and HC and NO_x emissions are recorded. A quasi-dimensional model, with mixtures containing 0%, 50% and 100% H_2, is used by Perini et al. [14] to study CO and NO emissions. The tests conducted by Ma et al. [15] using a supercharged engine contain mixtures with 0%, 30% and 55% H_2, and report only CO, HC and NO_x emissions.

* Corresponding author.
E-mail addresses: emilio.navarro@upm.es (E. Navarro), teresa.leo.mena@upm.es (T.J. Leo).

Nomenclature

a	crank radius, m; Vibe parameter
A	combustion chamber surface area, m^2; constant for induction time
A_s	throat area
C	constant of Woschni equation
c_D	discharge coefficient
c_p	specific thermal capacity at constant pressure, J mol^{-1} K^{-1}
C_1	constant of Woschni equation
C_2	constant of Woschni equation
CNG	compressed natural gas
D	cylinder bore, m
e	relative offset (cylinder axis offset from the crankshaft axis/crank radius)
E_a	constant for induction time
h	specific enthalpy, J kg^{-1}; convection heat-transfer coefficient, W/m^2 K
h_{cc}	equivalent height of the combustion chamber, m
HCNG	natural gas–hydrogen blend
H_2C	compressed hydrogen
H_2L	liquid hydrogen
K_P	equilibrium constant
L	piston stroke
m	mass, kg; constant of Woschni equation; shape parameter in Vibe equation
$\dot{m}$	mass flow rate
N	total mole number of products, mol
NG	natural gas
n	crankshaft rotational speed (rad/s, rpm); constant for induction time
p	pressure, kPa
p_m	motored cylinder pressure
p_r	inlet valve closing pressure
p_s	pressure at the throat
p_t	stagnation pressure
Q	heat transfer, J
$\dot{Q}$	heat transfer rate, W
r_c	compression ratio
R	universal gas constant, J mol^{-1} K^{-1}
R_g	gas constant, J kg^{-1} K^{-1}
S_P	mean piston velocity, m s^{-1}
t	time, s
T	temperature, K
T_r	inlet valve closing temperature
T_0	reference temperature, 298.15 K
u	specific internal energy
V	volume, m^3
V_d	displaced cylinder volume
V_r	inlet valve closing volume
x	burned mass fraction
y	instantaneous stroke, m
y_i	mole fraction of species i

Greek letters

β	hydrogen molar fraction in the mixture
ε	total mole number of fuel, mol
γ	thermal capacity ratio c_p/c_v
λ	ratio of connecting rod length to crank radius
ϕ	fuel/air equivalence ratio
η_{vg}	volumetric efficiency
τ	induction time, s
τ_{i0}	induction time, s
θ	crank angle, rad
θ_{ig}	spark timing
$\Delta\theta_c$	combustion development angle
v_i	mole amount of reactant i per mole of fuel mixture
μ_i	mole amount of product i per mole of fuel mixture
$\bar{\omega}$	molar humidity ratio

Subscripts

b	burned
c	cylinder, cylinder liner
ch	cylinder head
e	exit, exhaust
f	fuel
i	inlet; intake
p	piston crown
u	unburned
w	wall

Dimopoulos et al. [16] performed an experimental study of mixtures containing 0%, 5%, 10% and 15% H_2, but only determined CO, HC and NO_x.

Only recently are experimental studies reporting CO_2 emissions data being published. Park et al. [17] and Hu et al.[18] determined CO_2 emissions with 0%, 10%, 20%, 30% and 40% H_2 in the mixtures. Xu et al. [19] reported CO_2 emissions data for mixtures with an H_2 content of 0%, 15%, 20% and 25%. Ceper et al. [20] and Kahraman et al. [21] determined CO_2 emissions with 0%, 10%, 20% and 30% H_2 mixtures, whereas CO_2 from 30% H_2 mixtures is reported by Akansu and Bayrak [22]. These works show that emissions of hydrocarbons (HC), CO and CO_2 decrease significantly when hydrogen is used rather than pure natural gas. By using lean mixtures and optimizing spark timing, emissions can be lowered.

It was therefore deemed worthwhile to pay attention to CO_2 emissions, and to perform a quantitative study on the influence of the amount of hydrogen present in an HCNG mixture. This was regarded as a very interesting topic. As the studies reviewed in the literature covered the 0–30% H_2 range, a broader one would prove quite useful for discussing engine performance.

With these aims, the present study has developed a model of the engine cycle variations of a spark ignition engine fuelled by natural gas–hydrogen blends in order to analyse the influence of the hydrogen fraction on engine performance and CO_2 emissions. NO_x emissions are not presented because the kinetics of the combustion have not been considered, and most NO_x is produced by the oxidation of nitrogen formed in the combustion process.

2. Natural gas

With regard to emissions, natural gas is one of the cleaner fossil fuels existing today. It is therefore one of the alternatives under study for replacing oil. Nevertheless, certain properties of natural gas make spark ignition engine operation difficult. Its low flame propagation speed during combustion represents the main difficulty. This may be overcome by spark timing optimization, improvements in combustion chamber design, or by increasing turbulence [23,24].

Interest in natural gas can be evidenced by predicted increases in the number of serial vehicles manufactured using this fuel [25]. From 1991 to 2000, there was a 329% increase. From 2000 to the present, a 980% increase has been reported, and the trend continues to grow. Large increases are being recorded in Western Europe and Asia. In addition, it is interesting to consider the increase in the

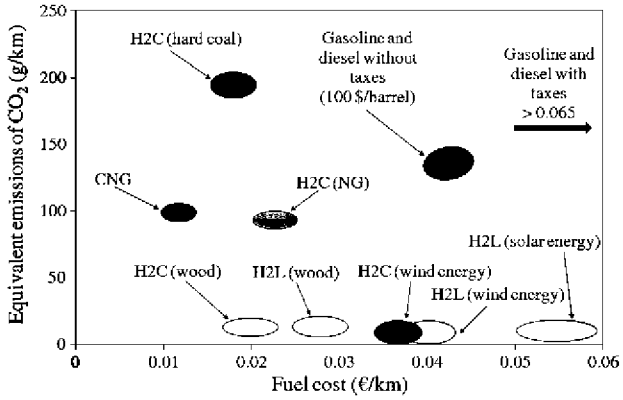

Fig. 1. Cost and CO_2 emissions for several fuels ([28] and data from the authors).

purchase cost of a vehicle using natural gas compared to those equipped with conventional engines. This varies from 10.1% to 13.2% for a vehicle equipped with a gasoline spark ignition engine with injection in the intake manifold [26,27]. Estimates have been made assuming production-line vehicle assembly.

Fuel costs and their relationship to equivalent CO_2 emissions are represented in Fig. 1 for several types of fuel ([28] and data from the authors).

As observed, the global CO_2 emissions associated with CNG and their costs are lower than those produced by gasoline or diesel. Hydrogen produces lower CO_2 emissions than CNG, gasoline or diesel, but hydrogen always originates from renewable sources. Due to the high price of crude oil, in some cases the cost of H_2 is lower than that of gasoline or diesel. In any case, this data has been prepared without taking into account the possible effects of an increase in demand or mass production.

3. Engine cycle simulation

A zero-dimensional model was chosen from the possible cycle simulation models indicated. It includes two regions at the combustion stage, for unburned and burned gases. The reason for this selection is based on the aim of this work: to perform parametric and optimization studies on various engines as a preliminary phase, prior to the development or modification process to make the engine operable with HCNG mixtures. Thus, it is important to avoid leaving a number of details to be changed later, such as the combustion chamber geometry.

The model used requires fewer fitting parameters than more complex models. However, this will not lead to worse results in this case. For example, those models using a turbulent combustion scheme to determine the burned mass fraction, usually based on the study performed by Blizard and Keck [29], require a large number of fitting parameters. When adopting literature values instead of performing the fitting process, the uncertainty of the results obtained increases. In addition, the combustion chamber geometry must be known in order to determine the front flame location and geometry by means of procedures such as those proposed by Bayraktar [30,31].

In the zero-dimensional model with two zones, each of these regions can be studied separately as two systems with a uniform composition and thermodynamic state. The geometry of both regions must be calculated to evaluate the heat transfer [32–35]. Models assuming similar hypotheses have been developed to study the behaviour of reciprocating engines with different pure fuels [36]. In this work, the fuel consists of a natural gas and hydrogen mixture with variable proportions.

To develop the model proposed [37], the following assumptions and approximations are considered:

1. The fluid under study behaves as an ideal mixture consisting of:
   a. Humid air, fuel and residual gases, during the intake and compression processes.
   b. Two regions, one corresponding to the unburned mixture (air, fuel and residual gases) and the other to the burned gases, during the combustion process.
   c. The combustion products, during the expansion process.
2. The fluid velocity inside the combustion chamber is negligible.
3. The blow-by effect is neglected.
4. Spherical front flame is assumed.
5. Uniform temperature is assumed in each region.
6. The determination of unburned gas properties is performed by neglecting the pre-flame reactions, assuming the gas is frozen (the gas consists of a mixture of ideal gases).
7. Local thermodynamic equilibrium is assumed, allowing the use of the ideal gas state equation with the burned and unburned gas [38].
8. The reactant gas mixture is at thermodynamic equilibrium.

3.1. Mixing and intake processes

The fuel is introduced in the intake manifold and mixed with air. The chemical equation of the process is

$$\begin{aligned}&\varepsilon\cdot\phi(v_1CH_4(g)+v_2H_2(g))_{(T_f,p_f)}+(0.21O_2+0.79N_2\\&\quad+\tilde{\omega}H_2O)_{(T_i,p_i)}\\&\rightarrow(0.21O_2+0.79N_2+\tilde{\omega}H_2O)_{(T,p)}+\varepsilon\cdot\phi\cdot(v_1CH_4(g)\\&\quad+v_2H_2(g))_{(T,p)}\end{aligned}\tag{1}$$

where ε is the total mole number of fuel, ϕ represents the fuel/air equivalence ratio, $\tilde{\omega}$ represents the molar humidity ratio, and v_i stands for the mole amount of component i per mole of fuel mixture. If pure natural gas is used, $v_2 = 0$, but $v_1 = 0$ if pure hydrogen is used.

The thermodynamic properties of the air–fuel mixture obtained are calculated by applying the first law of thermodynamics to the mixing process. Variations of kinetic and potential energies have been neglected, and no work is assumed during the process. The resulting equation to be solved is

$$\begin{aligned}&\sum_{n=1}^{N}\varepsilon\cdot\phi\cdot v_i\left[\int_{T_0}^{T}c_{p_i}^{o}(T)dT-\int_{T_0}^{T_f}c_{p_i}^{o}(T)dT\right]\\&+0.21\left[\int_{T_0}^{T}c_{p_{O_2}}^{o}(T)dT-\int_{T_0}^{T_i}c_{p_{O_2}}^{o}(T)dT\right]\\&+0.79\left[\int_{T_0}^{T}c_{p_{N_2}}^{o}(T)dT-\int_{T_0}^{T_i}c_{p_{N_2}}^{o}(T)dT\right]\\&+\tilde{\omega}\left[\int_{T_0}^{T}c_{p_{H_2O}}^{o}(T)dT-\int_{T_0}^{T_i}c_{p_{H_2O}}^{o}(T)dT\right]-Q\\&=0\end{aligned}\tag{2}$$

where $c_{p_i}^{0}$ represents the constant-pressure specific thermal capacity of gas i, considered an ideal gas [39], T_0 stands for the reference temperature (298.15 K), T_i is the intake air temperature, T_f represents the fuel temperature prior to injection, and Q is the heat transfer during the process.

Once the air–fuel mixture is obtained, it is introduced into the cylinder. This phase is characterized by the mixing process of the

Table 1
Woschni coefficients.

	Gas exchange	Compression	Combustion and expansion
C	3.26	3.26	3.26
m	0.8	0.8	0.8
C_1	6.18	2.28	2.28
C_2	0	0	3.24×10^{-3}

residual gases inside the cylinder and the air–fuel mixture entering in the cylinder.

To calculate the thermodynamic conditions during the gas exchange processes, the general equation to be solved is

$$\frac{dp_c}{dt} = \gamma_c p_c \left(\frac{\dot{m}_i}{m_c} \frac{\Delta h_i}{c_{p,c} T_c} - \frac{\dot{m}_e}{m_c} \frac{\Delta h_e}{c_{p,c} T_c} - \frac{\dot{V}_c}{V_c} \right) + \frac{dm_c}{dt} \frac{(c_{p,c} T_c - \Delta h_c)}{V_c} \times (\gamma_c - 1) - \frac{\dot{Q}}{V_c} (\gamma_c - 1) \tag{3}$$

where e stands for exhaust and i for intake. In this equation, γ_c, $c_{p,c}$ and V_c represent the thermal capacity ratio, constant-pressure specific thermal capacity and cylinder volume, respectively, $\dot{m}$ means mass flow rate, and $\dot{Q}$ stands for the heat transfer rate. In addition, the following equations must be used

$$\frac{dm_c}{dt} = \dot{m}_i - \dot{m}_e \tag{4}$$

and

$$\dot{m} = \begin{cases} c_D A_s \frac{p_t}{\sqrt{R_g \cdot T_t}} \left(\frac{p_s}{p_t} \right)^{\frac{1}{\gamma}} \sqrt{\frac{2\gamma}{\gamma - 1} \left[1 - \left(\frac{p_s}{p_t} \right)^{\frac{\gamma - 1}{\gamma}} \right]}, & \text{if} \quad \frac{p_t}{p_s} < \left(\frac{\gamma + 1}{2} \right)^{\frac{\gamma}{\gamma - 1}} \\ c_D A_s \frac{p_t}{\sqrt{R_g \cdot T_t}} \sqrt{\gamma} \left(\frac{2}{\gamma + 1} \right)^{\frac{\gamma + 1}{2(\gamma - 1)}}, & \text{if} \quad \frac{p_t}{p_s} \geqslant \left(\frac{\gamma + 1}{2} \right)^{\frac{\gamma}{\gamma - 1}} \end{cases} \tag{5}$$

where c_D is the discharge coefficient, A_s represents the throat area, and p_t and p_s stand for the stagnation pressure and the pressure at the throat, respectively.

Moreover, to evaluate the heat transfer rate, the convection heat transfer coefficient must be calculated. Therefore, similarly to the compression process detailed in the following section, the Woschni equation [40] is used (Eqs. (11) and (12) and Table 1).

3.2. Compression and expansion

For both the compression and expansion phases, the equations governing such processes are similar, except that the gas composition during the expansion process is variable due to the existence of dissociation reactions.

The thermodynamic conditions during the process are determined by applying the first law of thermodynamics to the fluid inside the cylinder. Variations of mechanical energy are neglected, and the equation of state for an ideal gas is used for the gas mixture. Then, dividing by the crank angle θ, the following expression can be written

$$\frac{dp}{d\theta} = -\gamma \frac{p}{V} \frac{dV}{d\theta} + \frac{\gamma - 1}{V} \frac{dQ}{d\theta} \tag{6}$$

The terms appearing in this equation are evaluated by means of the following expressions

$$\frac{dQ}{d\theta} = \frac{h(\theta) A(\theta) (T(\theta) - T_w)}{n} \tag{7}$$

where h and n stand for the convection heat-transfer coefficient and the crankshaft rotational speed, respectively. The wall temperature is represented by T_w. Total area A is the sum of the surface areas of cylinder liner A_c, cylinder head A_{ch} and piston crown A_p, respectively

$$A = A_c + A_{ch} + A_p = \pi D y + \frac{\pi D^2}{2} \tag{8}$$

which can be expressed as a function of cylinder bore D and instantaneous stroke y. This magnitude can be calculated by

$$y = h_{cc} + a \left[\sqrt{(2\lambda + 1)^2 - e^2} - \cos\theta - \sqrt{4\lambda^2 - (\sin\theta - e)^2} \right] \tag{9}$$

where h_{cc} is the equivalent height of the combustion chamber, and a, λ and e represent the crank radius, the ratio of connecting rod length to crank radius, and the relative offset (cylinder axis offset from the crankshaft axis/crank radius), respectively

$$h_{cc} = \frac{L}{r_c - 1} = \frac{a \left[\sqrt{(2\lambda + 1)^2 - e^2} - \sqrt{(2\lambda - 1)^2 - e^2} \right]}{r_c - 1} \tag{10}$$

where r_c stands for the compression ratio and L is the piston stroke.

As stated above, the convection heat transfer coefficient is calculated using the Woschni equation

$$h = C D^{m-1} p^m T^{0.75 - 1.62m} U^m \tag{11}$$

where

$$U = C_1 S_P + C_2 \frac{V_d T_r}{p_r V_r} (p - p_m) \tag{12}$$

where S_p is the mean piston velocity, V_d is the displaced cylinder volume, p_m is the motored cylinder pressure, and T_r, p_r and V_r represent the inlet valve closing temperature, pressure and volume, respectively.

The wall temperature [41] is evaluated by means of

$$T_w = 440 + 9\eta_{vg} (nD)^{0.2} \tag{13}$$

with η_{vg} being the volumetric efficiency.

Afterwards, Eqs. (6)–(13) lead to

$$\frac{dp}{d\theta} = -\gamma \frac{p}{V} \frac{dV}{d\theta} + \frac{\gamma - 1}{nV} \left[C D^{m-1} p^m T^{0.75 - 1.62m} \left(C_1 S_P + C_2 \frac{V_d T_r}{p_r V_r} (p - p_m) \right)^m \left(\pi D y + \frac{\pi D^2}{2} \right) [T - (440 + 9\eta_{vg} (nD)^{0.2})] \right] \tag{14}$$

which makes it possible to determine the fluid evolution during either the compression or expansion process.

3.3. Combustion

Ten chemical species [42,43] and two regions have been considered inside the chamber (unburned and burned gas regions) for the combustion process. The corresponding chemical reaction is

$$\begin{aligned} &\varepsilon\phi(\upsilon_1 CH_4 + \upsilon_2 H_2) + (0.21O_2 + 0.79N_2 + \tilde{\omega} H_2O) \\ &\quad \rightarrow \mu_1 CO_2 + \mu_2 H_2O + \mu_3 N_2 + \mu_4 O_2 + \mu_5 CO + \mu_6 H_2 + \mu_7 H \\ &\qquad + \mu_8 O + \mu_9 OH + \mu_{10} NO \end{aligned} \tag{15}$$

The mole amount of product i (i = 1,…,10) per mole of fuel mixture is represented by μ_i.

To solve this problem, a non-linear equation system is used, constituted by the mass balances

$$\begin{aligned} &C \rightarrow \varepsilon\phi\upsilon_1 = (y_1 + y_5)N \\ &H \rightarrow \varepsilon\phi(4\upsilon_1 + 2\upsilon_2) + 2\tilde{\omega} = (2y_2 + 2y_6 + y_7 + y_9)N \\ &O \rightarrow 0.42 + \tilde{\omega} = (2y_1 + y_2 + 2y_4 + y_5 + y_8 + y_9 + y_{10})N \\ &N \rightarrow 0.79 \cdot 2 = (2y_3 + y_{10})N \end{aligned} \tag{16}$$

and the equilibrium constants K_p corresponding to the dissociation of the products in equilibrium

$$\begin{aligned}
&\frac{1}{2}H_2 \rightleftarrows H \quad \rightarrow \quad K_1 = \frac{y_7 p^{1/2}}{y_6^{1/2}}\\
&\frac{1}{2}O_2 \rightleftarrows O \quad \rightarrow \quad K_2 = \frac{y_8 p^{1/2}}{y_4^{1/2}}\\
&\frac{1}{2}H_2 + \frac{1}{2}O_2 \rightleftarrows OH \quad \rightarrow \quad K_3 = \frac{y_9}{y_4^{1/2} y_6^{1/2}}\\
&\frac{1}{2}O_2 + \frac{1}{2}N_2 \rightleftarrows NO \quad \rightarrow \quad K_4 = \frac{y_{10}}{y_4^{1/2} y_3^{1/2}}\\
&H_2 + \frac{1}{2}O_2 \rightleftarrows H_2O \quad \rightarrow \quad K_5 = \frac{y_7}{y_4^{1/2} y_6 p^{1/2}}\\
&CO + \frac{1}{2}O_2 \rightleftarrows CO_2 \quad \rightarrow \quad K_6 = \frac{y_1}{y_4^{1/2} y_5 p^{1/2}}
\end{aligned} \tag{17}$$

where y_i is the mole fraction of species i in the products, and N is the total mole amount of the products. Then $\mu_i = y_i \cdot N$ and

$$\sum_{i=1}^{10} y_i = 1 \tag{18}$$

It must be noted that when pure hydrogen is used, $v_1 = 0$, $y_1 = 0$, $y_5 = 0$ and K_6 do not apply because carbon is not present in the medium.

The equilibrium constant values are calculated by means of the expression

$$\log K_p = A \ln \frac{T}{1000} + \frac{B}{T} + C + DT + ET^2 \tag{19}$$

where constants A, B, C, D and E are taken from Ferguson [43] and Olikara and Borman [44].

In addition, the first law of thermodynamics is used. Because the two regions (for unburned and burned gas) are assumed to be inside the combustion chamber, this equation can be written as

$$Q_u + Q_b - \int_1^2 p dV = [U_u + U_b]_2 - [U_u + U_b]_1 \tag{20}$$

where 1 and 2 represent the initial and final states at each step in the calculation, respectively.

Taking into account Eq. (7), in this case

$$Q_u = \frac{A_u h_u (T_u - T_{w,u})}{n} \Delta\theta \tag{21}$$

$$Q_b = \frac{A_b h_b (T_b - T_{w,b})}{n} \Delta\theta \tag{22}$$

where $\Delta\theta$ is the crank angle increment and

$$\int_1^2 p dV = \frac{p_2 + p_1}{2}(V_2 - V_1) \tag{23}$$

as well as the equations of state for unburned and burned gas, the following equation is obtained

$$\left[\frac{A_u h_u \left(\frac{pV_u}{n_u R} - T_{w,u}\right)}{n} + \frac{A_b h_b \left(\frac{pV_b}{n_b R} - T_{w,b}\right)}{n}\right] \Delta\theta - \frac{p_2 + p_1}{2}(V_2 - V_1) = (m_u u_u)_2 - (m_u u_u)_1 - (m_b u_b)_2 - (m_b u_b)_1 \tag{24}$$

where u means specific internal energy.

Similarly to the compression process, the Woschni expression, Eqs. (11) and (12), and Table 1 are used to calculate the heat transfer coefficient, and the Muller expression [41], Eq. (13), is used to calculate the cylinder wall temperature.

To calculate the volumes occupied by both unburned and burned gas, the mass inside the cylinder is considered constant. In addition, the Livengooz hypothesis [45] is used for the unburned gas

Table 2
Coefficients for the Eq. (34).

	A	E_a	n
H_2	2.82×10^{-13}	336	−1.3
CH_4	3.23×10^{-2}	192	−2.1

Table 3
Engine specifications.

Item	Value
Displacement volume (cm^3)	1039
Compression ratio	10.5
Bore (mm)	105
Stroke (mm)	120
Rating power (kW)	154
Rating torque (Nm)	620
Intake valve open (°BTDC)	18
Intake valve close (°ABDC)	37
Exhaust valve open (°BBDC)	56
Exhaust valve close (°ATDC)	11
Ratio of connecting rod length to crank radius	1.833
Relative offset	0.0422

Table 4
Engine operating conditions.

Case	n (rpm)	p_i (bar)	%H_2	ϕ	θ_{ig} (°)
A	1600	0.70	20	0.769	26
B	1600	1.20	20	0.769	26
C	1200	1.05	10	0.752	30
D	1200	1.05	30	0.714	30
E	1600	0.87	40	0.833	24
F	1600	0.65	50	0.800	22
G	2400	0.80	0	0.769	32
H	1200	1.05	0	0.613	30

$$pV_u^{\gamma_u} = p_{initial} V_{initial}^{\gamma_u} \tag{25}$$

where $p_{initial}$ and $V_{initial}$ represent the starting combustion pressure and volume, respectively.

Then

$$V_b = V - (1 - x) V_{initial} \left(\frac{p_{initial}}{p}\right)^{\frac{1}{\gamma_u}} \tag{26}$$

$$V_u = V - V_b \tag{27}$$

Burned mass fraction x is evaluated by integrating the Vibe function [46]

$$\frac{dx}{d\theta} = \frac{\theta}{\Delta\theta_c}(m+1) y^m \exp^{-a y^{(m-1)}} \tag{28}$$

where $\Delta\theta_c$ is the combustion development angle. Therefore

$$x = \int \frac{dx}{d\theta} d\theta = 1 - \exp^{-a y^{(m+1)}} \tag{29}$$

where m is the shape parameter ($m = 2$) and a stands for the Vibe parameter ($a = 5$).

The expressions used to evaluate the wet chamber surface areas for unburned gas A_u and burned gas A_b are the following

$$A_u = (1 - x) A \tag{30}$$

$$A_b = xA \tag{31}$$

3.4. Knock

Knock is an important effect to consider for poly-fuel engines. The appearance of knock has been determined by using empirical

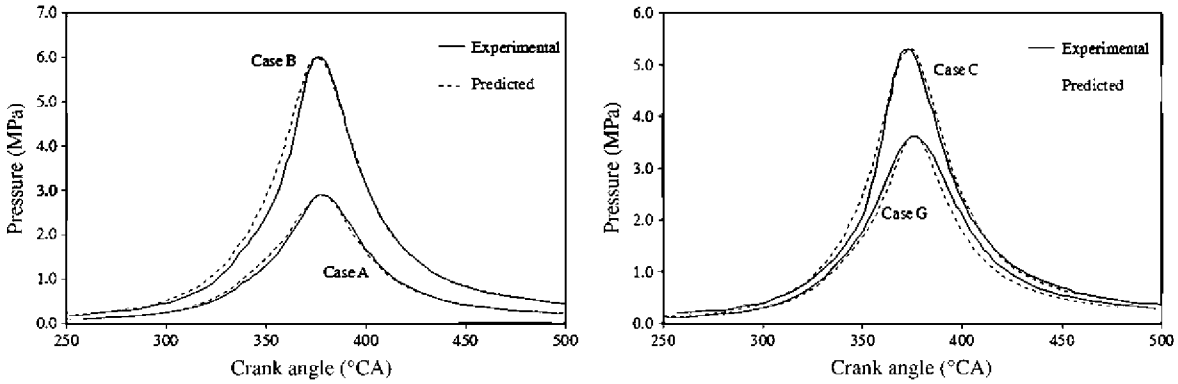

Fig. 2. Indicated cycle obtained using the model, compared to experimental data [10] (cases A, B, C and G).

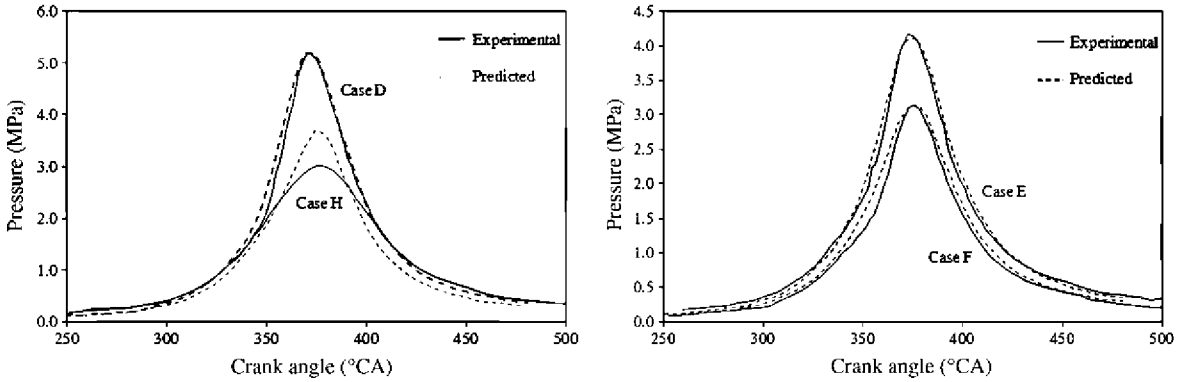

Fig. 3. Indicated cycle obtained using the model, compared to experimental data [10] (cases D, H, E and F).

Table 5
Engine operating conditions.

Item	Value
Ambient temperature (K)	294.15
Fuel temperature (K)	294.15
Intake pressure (bar)	0.8
Exhaust pressure (bar)	1.0
Fuel/air equivalence ratio	0.833
Spark timing (°)	17
Speed engine (rpm)	2000

models to calculate induction time τ_{i0}. This is calculated from pure methane and hydrogen induction times by means of the following expression [47]

$$\tau_{i0} = \tau_{CH_4}^{1-\beta} \cdot \tau_{H_2}^{\beta} \tag{32}$$

where

$$\tau = A \cdot \left(\frac{p}{T}\right)^{n} \cdot \exp\left(\frac{E_a}{RT}\right) \tag{33}$$

where p, T and β stand for pressure, temperature, and the hydrogen molar fraction in the mixture, respectively. The values of parameters A, n and E_a, depending on the fuel, are shown in Table 2.

Therefore

$$\tau_{i0} = A_{H_2}^{\beta} \cdot A_{CH_4}^{(1-\beta)} \cdot \left(\frac{p}{T}\right)^{n_{H_2}\beta + n_{CH_4}(1-\beta)} \cdot \exp\left(\frac{E_{H_2}\beta + E_{CH_4}(1-\beta)}{RT}\right) \tag{34}$$

Knock appears when the following condition is attained

$$\int_0^t \frac{1}{\tau_{i0}(t)} dt = 1 \tag{35}$$

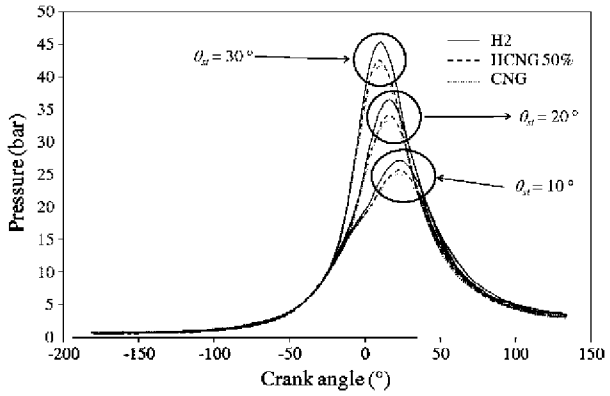

Fig. 4. Variation of pressure as a function of the crank angle, fuel composition and spark timing.

4. Validation of the model

The experimental results provided by Ma et al. [10], obtained under given operating conditions, have been used to validate the model. Therefore, the operating conditions imposed in this study [10] have been used (see Table 4 of this reference); the experimental results used for validation purposes are shown in Fig. 8 of the same reference, and the specifications of the engine used by Ma et al. [10] are detailed in Refs. [48,10]. Thus, the specifications of the engine simulated in this work are compiled in Table 3, and the different operating conditions used to validate the model are shown in Table 4, where θ_{ig} represents the spark timing crank angle and ϕ stands for the fuel/air equivalence ratio.

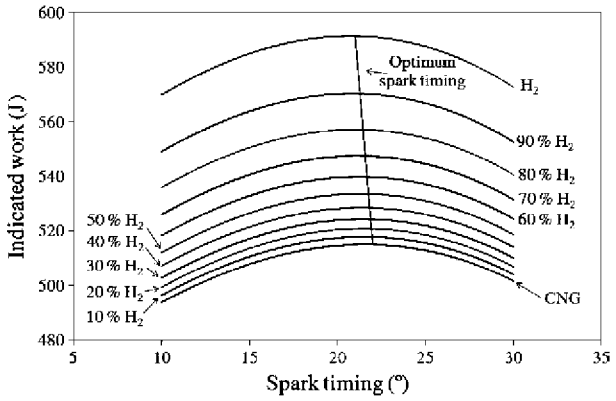

Fig. 5. Indicated work as a function of the spark timing and fuel composition.

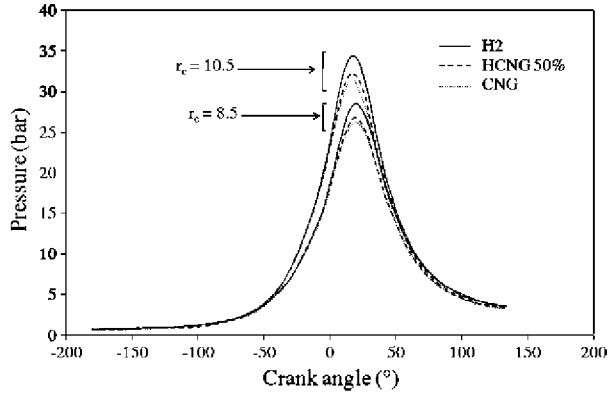

Fig. 6. Variation of pressure as a function of the crank angle, fuel composition and compression ratio.

Figs. 2 and 3 show the evolution of pressure as a function of crank angle for both experimental and calculated data, in each case. There are two main error sources in cases A to G: some parameters of the actual engine are unknown, and have been adjusted to obtain the best approximation and blow-by effect. In case H, the difference between experimental and calculated data is larger. As shown in Table 4, this case corresponds to pure natural gas, and the fuel/air equivalence ratio is 0.613, very close to the lower operating limit, where combustion is unstable and incomplete. This is not considered by the model. In cases A to G, the model fits the experimental pressure data with an error lower than 3%.

5. Results and discussion

5.1. Effect of hydrogen addition on engine performance

In order to evaluate the influence of the hydrogen fraction on engine performance, different fuels are used to run the model. The specifications of the simulated engine are shown in Table 3, and the operating conditions in Table 5.

Fig. 4 shows variations in pressure with respect to the crank angle for three mixtures (pure natural gas, HCNG with 50% hydrogen, and pure hydrogen) and different spark timing values. Fig. 5 shows the indicated work as a function of spark timing. Fig. 6 shows variations in pressure with respect to the crank angle for the three mixtures and different compression ratio values. Fig. 7 represents the power delivered by each fuel as a function of the crankshaft engine rotational speed.

As shown in Figs. 4 and 5, the maximum pressure in the cylinder and the indicated work increase as the hydrogen fraction rises. The maximum pressure is 8% higher with pure hydrogen than with pure CNG. Consequently, the indicated work and power delivered are also enhanced by increasing the amount of hydrogen. The indicated work is 15.2% higher with pure hydrogen than with pure CNG. This occurs because the specific energy of hydrogen is higher than that of natural gas. Therefore, the temperature reached in the cylinder is also higher. As observed in Fig. 4, the crank angle at which the maximum pressure occurs is different for each fuel.

Fig. 5 shows the optimum spark timing required to attain the maximum work depending on the hydrogen content of the mixture.

Similar behaviour to that described earlier is observed at two different compression ratios (see Fig. 6). The maximum pressure rises as the hydrogen content of the mixture increases. An analogous trend is observed for the power delivered as a function of the engine speed (Fig. 7). As in the case of the indicated work, the power increase is proportional to the increase in hydrogen content, exhibiting a nonlinear variation with the hydrogen content in the mixture.

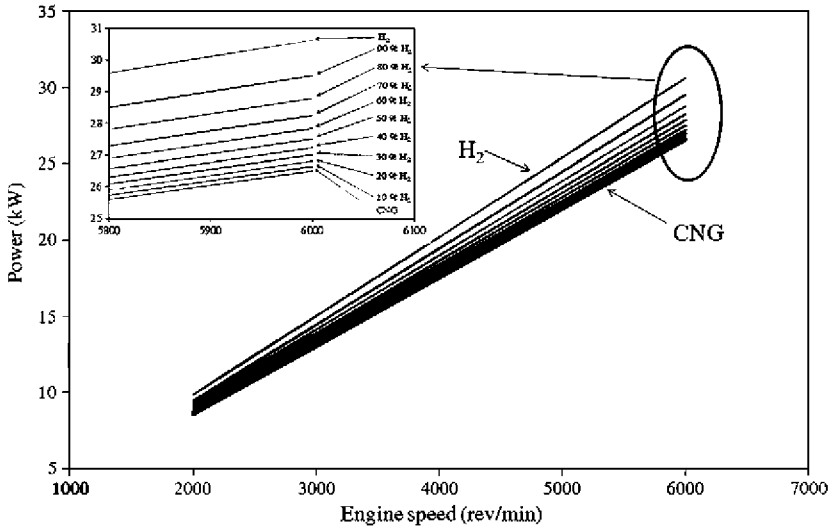

Fig. 7. Power delivered by the engine as a function of the crankshaft rotational speed and fuel composition.

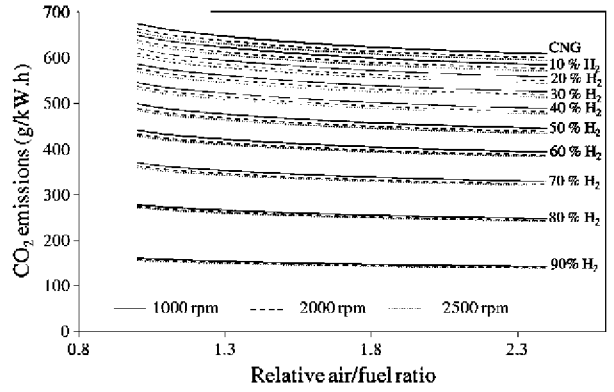

Fig. 8. CO_2 emissions as a function of the relative air/fuel ratio, fuel composition and crankshaft rotational speed.

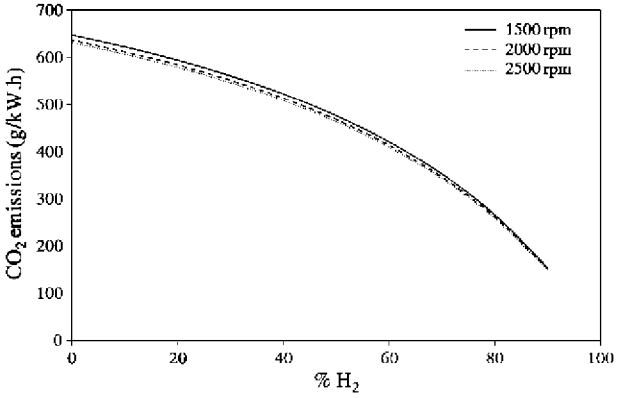

Fig. 9. CO_2 emissions as a function of the fuel composition and crankshaft rotational speed (relative air/fuel ratio = 1.3).

5.2. Effect of hydrogen addition and air/fuel ratio on CO_2 emissions

To analyse the effect of hydrogen addition and air/fuel ratio on CO_2 emissions, several blends of natural gas and hydrogen were studied: compressed natural gas (CNG), and HCNG with hydrogen fractions from 10% to 90%, with an air/fuel ratio within reasonable operating limits. Hydrogen has a high flame propagation speed and low ignition energy, making it possible to work with leaner mixtures than pure natural gas.

There is a limit for lean air–fuel mixtures because if this limit is reached, the combustion becomes unstable and incomplete. Operating close to this limit decreases the combustion speed and increases the ignition energy of the air–fuel mixture, leading to large cycle-by-cycle variations, thus decreasing the thermal efficiency.

Fig. 8 shows specific CO_2 emissions with respect to the air/fuel ratio for different fuel compositions at three different engine speeds, respectively. It is observed that specific CO_2 emissions decrease when fuel mixtures with increasing hydrogen content are used, when the air/fuel ratio increases, and when the crankshaft rotational speed increases.

A decrease in specific CO_2 emissions with an increasing H_2 content in the fuel mixture can be attributed to a progressive decrease in the carbon content, and also to the enhancement of the combustion process.

To explain the observed behaviour of CO_2 emissions with increasing air/fuel ratios, several aspects must be considered. The equilibrium temperature of the combustion products will decrease as the air/fuel ratio increases, with the maximum temperature value corresponding to an air/fuel ratio near the stoichiometric ratio. This affects the efficiency, which increases with higher air/fuel ratios. This occurs because the burned gas temperatures drop after combustion, thus decreasing the thermal capacities of the burned gas, and therefore increasing the effective value of the thermal capacity ratio in the expansion stroke. Efficiency increases due to the burned gas expand through a higher temperature increment before the exhaust. Then the expansion stroke work increases by mass fuel unit.

It must also be noted that the mean effective pressure diminishes with increasing air/fuel ratios. Although the efficiency increases, such an increase is balanced by the increase in the air/fuel ratio, and the latter has a greater influence. Fig. 8 shows that because both the power and the CO_2 emissions decrease as the air/fuel ratio increases, the latter exhibits greater drops, eventually leading to a decrease in specific CO_2 emissions. As an example, for 50% mixtures at 2000 rpm, power increases of 9.7% with respect to CNG are reached under the conditions studied, and reductions of up to 25.9% in specific CO_2 emissions are attained.

The behaviour caused by rotational speed variation can be justified based on the effect of the temperature reached inside the cylinder and its effect on CO_2 emissions. As the rotational speed increases, the engine behaves in a more adiabatic way. The temperature inside it rises, leading to lower CO_2 emissions with a more complex burned gas composition, in which species such as OH, O and H are present. In this case, power increases and CO_2 emissions decrease, leading to a clear drop in specific CO_2 emissions.

It is important to note that, as observed for the power increase, the drop in CO_2 shows a nonlinear variation as the hydrogen content increases. This can be seen in Fig. 9, which shows the case of a relative air/fuel ratio equal to 1.3. This is an important feature when selecting the optimum hydrogen content in the mixture, as lower proportions of hydrogen lead to smaller drops in CO_2 and smaller increases in power. As the hydrogen content increases, these phenomena are much more significant, becoming evident from 40% H_2 onwards. In any case, other factors must be considered, such as fuel costs, the cost of modifying the required engine, engine maintenance costs, and the safety problems that arise when the H_2 content is increased. Determining the optimum proportion of H_2 in the mixture therefore becomes a complex task, depending on the generation technologies (W-t-W studies) and their cost.

6. Conclusions

Given the growing importance of alternative fuels, an indicated cycle model for a spark ignition engine operating with variable blends of hydrogen and natural gas (HCNG) has been developed. This model makes it possible to modify geometrical parameters, engine operating conditions, and fuel composition. The model was used to determine the engine's performance and CO_2 emissions, and was experimentally validated, always producing mean indicated pressure errors under 3%. The maximum cycle pressure and indicated work obtained increase along with the proportion of hydrogen in the HCNG, and leaner mixtures can be used. As the hydrogen content in the mixture rises, CO_2 emissions drop. The decrease in CO_2 emissions and the increase in power both exhibit a nonlinear variation as the hydrogen content rises, and these phenomena are much more significant when the hydrogen content in the mixture is high. This, along with the resulting increase in power, makes HCNG advantageous compared to other fuels.

Acknowledgement

This work has been partially supported by the Universidad Politécnica de Madrid within the framework of Project Code No. AL11-P(I+D)-03.

References

[1] Wua X, Daniel R, Tian G, Xu H, Huang Z, Richardson D. Dual-injection: the flexible, bi-fuel concept for spark-ignition engines fuelled with various gasoline and biofuel blends. Appl Energy 2011;88:2305–14.

[2] Liang C, Ji C, Liu X. Combustion and emissions performance of a DME-enriched spark-ignited methanol engine at idle condition. Appl Energy 2011;88:3704–11.

[3] Mancaruso E, Vaglieco BM. Premixed combustion of GTL and RME fuels in a single cylinder research engine. Appl Energy 2012;91:385–94.

[4] Visakhamoorthy S, Tzanetakis T, Haggith D, Sobiesiak A, Wen JZ. Numerical study of a homogeneous charge compression ignition (HCCI) engine fueled with biogas. Appl Energy 2012;92:437–46.

[5] Machrafi H, Cavadias S, Amouroux J. A parametric study on the emissions from an HCCI alternative combustion engine resulting from the auto-ignition of primary reference fuels. Appl Energy 2008;85:755–64.

[6] BP Statistical Review of World Energy; 2011. <http://www.bp.com/liveassets/bp_internet/globalbp/globalbp_uk_english/reports_and_publications/statistical_energy_review_2011/STAGING/local_assets/spreadsheets/statistical_review_of_world_energy_full_report_2011.xls> (accessed November 2011).

[7] U.S. Department of Energy. Transportation energy data book. <http://cta.ornl.gov/data/index.shtml> (accessed November 2011).

[8] White CM, Steeper RR, Lutz AE. The hydrogen-fueled internal combustion engine: a technical review. Int J Hydrogen Energy 2006;31:1292–305.

[9] Ji C, Wang S, Zhang B. Performance of a hybrid hydrogen–gasoline engine under various operating conditions. Appl Energy, in press. Corrected proof. <http://dx.doi.org/10.1016/j.apenergy.2011.11.056>.

[10] Ma F, Wang Y, Wang M, Liu H, Wang J, Ding S, et al. Development and validation of a quasi-dimensional combustion model for SI engines fuelled by HCNG with variable hydrogen fractions. Int J Hydrogen Energy 2008;33:4863–75.

[11] Park J, Cha H, Song S, Chun KM. A numerical study of a methane-fuelled gas engine generator with addition of hydrogen using cycle simulation and DOE method. Int J Hydrogen Energy 2001;36:5153–62.

[12] Dimopoulos P, Rechsteiner C, Soltic P, Laemmle C, Boulouchos K. Increase of passenger car engine efficiency with low engine-out emissions using hydrogen-natural gas mixtures: a thermodynamic analysis. Int J Hydrogen Energy 2007;32:3073–83.

[13] Bysveen M. Engine characteristics of emissions and performance using mixtures of natural gas and hydrogen. Energy 2007;32:482–9.

[14] Perini F, Paltrinieri F, Mattarelli E. A quasi-dimensional combustion model for performance and emissions of SI engines running on hydrogen-methane blends. Int J Hydrogen Energy 2010;35:4687–701.

[15] Ma F, Wang M, Jiang L, Deng J, Chen R, Naeve N, et al. Performance and emission characteristics of a turbocharged spark-ignition hydrogen-enriched compressed natural gas engine under wide open throttle operating conditions. Int J Hydrogen Energy 2010;35:12502–9.

[16] Dimopoulos P, Bach C, Soltic P, Boulouchos K. Hydrogen-natural gas blends fuelling passenger car engines: combustion, emissions and well-to-wheels assessment. Int J Hydrogen Energy 2008;33:7224–36.

[17] Park C, Kim C, Choi Y, Won S, Moriyoshi Y. The influences of hydrogen on the performance and emission characteristics of a heavy duty natural gas engine. Int J Hydrogen Energy 2011;36:3739–45.

[18] Hu E, Huang Z, Liu B, Zheng J, Gu X, Huang B. Experimental investigation on performance and emissions of a spark-ignition engine fuelled with natural gas–hydrogen blends combined with EGR. Int J Hydrogen Energy 2009;34:528–39.

[19] Xu J, Zhang X, Liu J, Fan L. Experimental study of a single-cylinder engine fueled with natural gas–hydrogen mixtures. Int J Hydrogen Energy 2010;35:2909–14.

[20] Ceper BA, Akansu SO, Kahraman N. Investigation of cylinder pressure for H2/CH4 mixtures at different loads. Int J Hydrogen Energy 2009;34:4855–61.

[21] Kahraman N, Ceper B, Akansu SO, Aydi K. Investigation of combustion characteristics and emissions in a spark ignition engine fuelled with natural gas–hydrogen blends. Int J Hydrogen Energy 2009;34:1026–34.

[22] Akansu SO, Bayrak M. Experimental study on a spark ignition engine fuelled by CH_4/H_2 (70/30) and LPG. Int J Hydrogen Energy 2011;36:9260–6.

[23] Sen AK, Wang J, Huang Z. Investigating the effect of hydrogen addition on cyclic variability in a natural gas spark ignition engine: wavelet multiresolution analysis. Appl Energy 2011;88:4860–6.

[24] Sen AK, Zheng J, Huang Z. Dynamics of cycle-to-cycle variations in a natural gas direct-injection spark-ignition engine. Appl Energy 2011;88:2324–34.

[25] IANGV, International association for natural gas vehicles. <http://www.iangv.org/stats/NGV_Statistics10_files/sheet007.htm#RANGE!A1> (accessed November 2011).

[26] Concawe/Eucar/JRC, Well-To-Wheels analysis of future automotive fuels and powertrains in the European context. Report 2007. <http://iet.jrc.ec.europa.eu/about-jec/> (accessed November 2011).

[27] General Motors Corporation. Well-to-wheels analysis of advanced fuel/vehicle systems -a north american study of energy use, greenhouse gas emissions, and criteria pollutant emissions; 2005. <http://www.transportation.anl.gov/pdfs/TA/339.pdf> (accessed November 2011).

[28] Wurster R. H2-based road transport in comparison. In: Proceedings of DIME international conference "innovation, sustainability and policy". Bordeaux, France; 2008. ,http://www.lbst.de/ressources/docs2008/DIME-Conference_H2-AutomotiveFuel_LBST_11SEP2008_V4.pdf>.

[29] Blizard NC, Keck JC, Experimental and theoretical investigation of turbulent burning model for internal combustion engines. SAE Paper 1974, 740191.

[30] Bayraktar H. Theoretical investigation of using ethanol-gasoline blends on SI engine combustion and performance. Ph.D. thesis, Karadeniz Technical University, Trabzon, Turkey; 1997.

[31] Bayraktar H. Theoretical investigation of flame propagation process in an SI engine running on gasoline–ethanol blends. Renew Energy 2007;32:758–71.

[32] Kang K, Spng NW. Cycle simulation for a spark ignition engine using a turbulent combustion model. SAE paper, 872154; 1987.

[33] Bascunana JL. Burning rate development in a closed vessel of arbitrary shape and variable volume, for variable but uniform pressure. Trans ASME J Eng Power 1969;91A:69–71.

[34] Gatowski A, Balles EN, Chun KM, Nelson FE, Ekchian JA, Heywood JB. Heat release analysis of engine pressure data. SAE paper, 841359; 1984.

[35] Verhelst S, Sheppard CGW. Multi-zone thermodynamic modelling of spark-ignition engine combustion – an overview. Energy Convers Manage 2009;50:1326–35.

[36] Caton JA. Implications of fuel selection for an SI engine: results from the first and second laws of thermodynamics. Fuel 2010;89:3157–66.

[37] Navarro E, Varela E. Descomposición en serie de la presión generada por la combustión en Motores Alternativos. Anal Ingeniería Mecánica 1992;9:45–9. ISSN: 0212–5072.

[38] Kempinski JM. Knock in spark ignition engines. SAE paper, 810147; 1981.

[39] Poling BE, Prausnitz JM, O'Connell JP. The properties of gases and liquids. 5th ed. New York: McGraw-Hill; 2001.

[40] Woschni G. A universal applicable equation for the instantaneous heat transfer coefficient in the internal combustion engine. SAE paper, 670931; 1967.

[41] Müller H, Bertling H. Programmierte Auswertung von Druckverläufen in Ottomotoren. Düsseldorf: VDI-Verlag; 1971.

[42] Svehla RA, McBride BH. Fortran IV computer program for calculation of thermodynamics and transport properties of complex chemical systems. NASA TN D-7056; 1973.

[43] Ferguson CR. Internal combustion engines: applied thermosciences. New York: John Wiley & Sons; 1986.

[44] Olikara C, Borman GL. a computer program for calculating properties of equilibrium combustion products with some applications to I.C. engines. SAE paper, 750468; 1975.

[45] Livengood JC, Taylor CF, Wu PC. Measurement of gas temperature in an engine by the velocity of sound method. SAE paper, 580064; 1958.

[46] Vibe II. Brennverlauf und Kreisprozess von Verbrennungsmotoren. Berlin: Verlag Technik; 1970.

[47] Gersen S. Experimental study of the combustion properties of methane/hydrogen mixtures. M Sc Thesis, University of Groningen; 2007.

[48] Ma F, Wang Y, Liu HLY, Wang J, Ding S. Effects of hydrogen addition on cycle-by-cycle variations in a lean burn natural gas spark-ignition engine. Int J Hydrogen Energy 2008;33:823–31.